Eur. J. Mineral., 35, 1079–1090, 2023
https://doi.org/10.5194/ejm-35-1079-2023

European Journal of Mineralogy
Open Access

Electron backscatter diffraction analysis combined with NanoSIMS U–Pb isotope data reveal intra-grain plastic deformation in zircon and its effects on U–Pb age: examples from Himalayan eclogites, Pakistan

Hafiz U. Rehman[1], Takanori Kagoshima[2,3], Naoto Takahata[2], Yuji Sano[2,4], Fabrice Barou[5], David Mainprice[5], and Hiroshi Yamamoto[1]

[1]Graduate School of Science and Engineering, Kagoshima University, Kagoshima, 890-0065, Japan
[2]Atmosphere and Ocean Research Institute, The University of Tokyo, Kashiwa, 277-8564, Japan
[3]Graduate School of Science and Engineering, University of Toyama, Toyama, 930-8555, Japan
[4]Center for Advanced Marine Core Research, Kochi University, Kochi, 783-8502, Japan
[5]Géosciences Montpellier UMR CNRS 5243, Université de Montpellier, Montpelier, 34095, France

Correspondence: Hafiz U. Rehman (hafiz@sci.kagoshima-u.ac.jp)

Received: 30 January 2023 – Revised: 27 September 2023 – Accepted: 18 October 2023 – Published: 5 December 2023

Abstract. Zircon grains preserve records of crystallization, growth, and/or deformation that can be envisaged from their internal structures and through the U–Pb isotope analysis. Electron backscatter diffraction (EBSD) is a non-destructive method for visualizing undeformed domains to differentiate them from those that are plastically deformed. In this study, we report EBSD analyses conducted on zircon grains, in thin sections with available textural information, from Himalayan eclogites. The studied eclogite samples show no petrographic evidence of shearing or mylonitization. However, several zircon grains preserve plastically deformed domains. These deformed domains display several degrees of misorientation relative to the undeformed domain and yielded geologically reset ages when analysed for U–Pb isotope ratios using nanoscale secondary ion mass spectrometry (NanoSIMS), in contrast to most undeformed domains which retained the protolith age. The degree of resetting is positively correlated with the extent of misorientation. These pieces of evidence indicate that plastic deformation in zircon grains, equilibrated at higher pressure–temperature conditions, affected the primary geochemical and geochronological records. Based on these observations, we assume that not only regional shearing/mylonitization in metamorphic rocks affects the geochemical records, but also that zircon grains in apparently unsheared high-grade metamorphic rocks behave plastically. The micro-scale intra-grain plastically deformed domains can easily be identified through EBSD analysis in the form of crystallographic misorientations. To extract meaningful geochronological results, it is necessary to identify undisturbed domains in zircon grains before applying any destructive analytical method.

1 Study background

Zircon, a common accessory mineral of igneous and metamorphic rocks, is highly resistant to alteration and preserves geochemical and geochronological records of its magmatic crystallization and growth or recrystallization during metamorphic events (Belousova et al., 2002; Cherniak and Watson, 2003). Backscattered electron (BSE) and cathodoluminescence (CL) images followed by direct isotopic measurements and trace-element analyses on polished surfaces of zircon grains have allowed the majority of earth scientists to understand the magma source of igneous rocks from which the zircon grains crystallized and to elucidate the thermal and deformational regimes of the metamorphic rocks in which the metamorphic domains of zircons overgrew or recrystallized. However, the existence of tiny (micro-scale)

deformed or geochemically reset domains is sometimes impossible to identify through the commonly used methods (e.g. optical microscopy, BSE, and CL imaging). Several studies have reported crystal plastic deformation in zircon grains in highly sheared metamorphic rocks (e.g. Reddy et al., 2006, 2007, 2009; Kusiak et al., 2013; Kovaleva and Klötzli, 2017; Kovaleva et al., 2021). Such shearing or deformation events in the host rocks reset the geochemical (redistribution of trace elements and isotopes) and geochronological records in zircon grains. Investigating such zircon grains using the electron backscatter diffraction (EBSD) method has proved that strain at low-angle boundaries, tilt dislocation, and rotation axis were the common mechanisms of deformation that disturbed the geochemical and geochronological records in zircon grains (e.g. Piazolo et al., 2012; Kovaleva et al., 2017, 2018). Some of the above-mentioned authors found plastically deformed zircon grains in shear zones or strongly foliated metamorphic rocks such as amphibolites, which were identified through EBSD analysis or transmission electron microscopy (TEM). However, little or no information exists on the strain regime of plastically deformed zircon in high-pressure metamorphic rocks such as eclogites. Focusing on eclogite, the aim of this study is to identify undeformed zircon domains retaining pristine information (from their protolith-related magmatic crystallization) and to compare them to micro-scale plastically deformed ones (growth/recrystallization or reset during their metamorphism and exhumation). The studied zircon grains were identified within thin sections, with available textural information, from Himalayan eclogites exposed in the Kaghan Valley, Pakistan. The target grains were investigated through optical microscopy, followed by BSE and CL imaging to identify deformation structures like fractures, resorption, bending, and presence of inclusions. Following those procedures, several selected grains were then investigated via EBSD for internal micro-textures at single-grain scale. Various domains were then analysed for multiple spots of U–Pb isotopic measurements using nanoscale secondary-ion mass spectrometry (NanoSIMS). The purpose was to elucidate the effect of plastic deformation on the U–Pb isotope system in zircon grains in eclogite. The data reveal several plastically deformed domains in the investigated zircon grains and that the geochronological record of these domains is affected, in contrast to the undeformed domains.

2 Geological description

Himalayan eclogites from the Kaghan Valley, Pakistan (Fig. 1), were investigated in this study. A previous study (Rehman et al., 2008) classified the Himalayan eclogites into high-pressure (HP) termed as Group I eclogites (with no coesite reported) and ultrahigh-pressure (UHP) termed as Group II eclogites (coesite-bearing). Protoliths of both groups were regarded as the Panjal Trap basalts (according to the concordant U–Pb age values of ca. 267.1 ± 2.4 Ma obtained from igneous zircon), which extruded widely along the northern margin of the Indian Plate and within the Tethys Ocean during the Permian time (Spencer et al., 1995; Rehman et al., 2013a, 2016). Later, during the India–Asia collision and subsequent subduction of the Indian Plate, the subducted continental crust, including the mafic Panjal Traps, formed HP and UHP eclogites in the Eocene (according to the concordant U–Pb age values of ca. 44.9 ± 1.2 Ma obtained from coesite-bearing metamorphic zircon; O'Brien et al., 2001; Kaneko et al., 2003; Rehman et al., 2013a, 2017).

Petrographically, both Group I and II eclogites show omphacite–garnet–quartz/coesite–rutile with rare phengite as the typical eclogite-facies assemblage and hornblende–epidote–titanite and quartz–diopside–albite symplectites as retrogression-related assemblages (Fig. 2). Extensive research work on the Kaghan Valley eclogites (e.g. field features, petrographic evidence, whole-rock and mineral geochemistry, conventional geothermobarometry based on elemental exchange in main mineral assemblages, and some trace-element thermometry) has been reported by, for example, Spencer et al. (1995), O'Brien et al. (2001), Kaneko et al. (2003), Wilke et al. (2010), Rehman (2019), and Rehman et al. (2007, 2008, 2018, 2019). Therefore, only brief information relevant to this study is presented here. Conventional geothermobarometry data revealed pressure–temperature (P–T) conditions of 2.33 ± 0.40 GPa and 766 ± 107 °C from Group I eclogites, 2.86 ± 0.04 GPa and 762 ± 46 °C from Group II eclogites (Rehman et al., 2007, 2013b), and 2.7 GPa at around 700 °C from coesite-bearing UHP gneisses (Kaneko et al., 2003). Trace-element thermometry (Ti-in-zircon and Zr-in-rutile) also yielded comparable temperatures of metamorphic equilibration for the Himalayan eclogites (Rehman et al., 2016, 2019).

3 Description of zircon grains

In this study, five zircon grains from two thin sections of Group I (HP) eclogites were investigated. Zircon grains in Group I eclogites exhibit irregular shapes (Fig. 2), are comparatively large, are optically pink, and range in size from 100 to 250 µm (some reach 500 µm), with rare oscillatory zoning, but the majority of grains lack specific zoning pattern when observed under CL spectroscopy (Fig. 3). In contrast, zircon grains in Group II eclogites are relatively small, white or colourless, mostly oval or euhedral, and preserve sector or fir tree zoning, typical for metamorphic zircon (details on the two zircon groups are reported in Rehman et al., 2013a). Past geochronological work on zircon grains in Group I eclogites revealed ^{235}U–^{207}Pb age values in the range 276 ± 1 Ma to 244 ± 11 Ma (see Rehman et al., 2013a). Most of those zircons were interpreted as magmatic, based on their relatively high Th/U ratios (> 0.3) and oscillatory zoning in

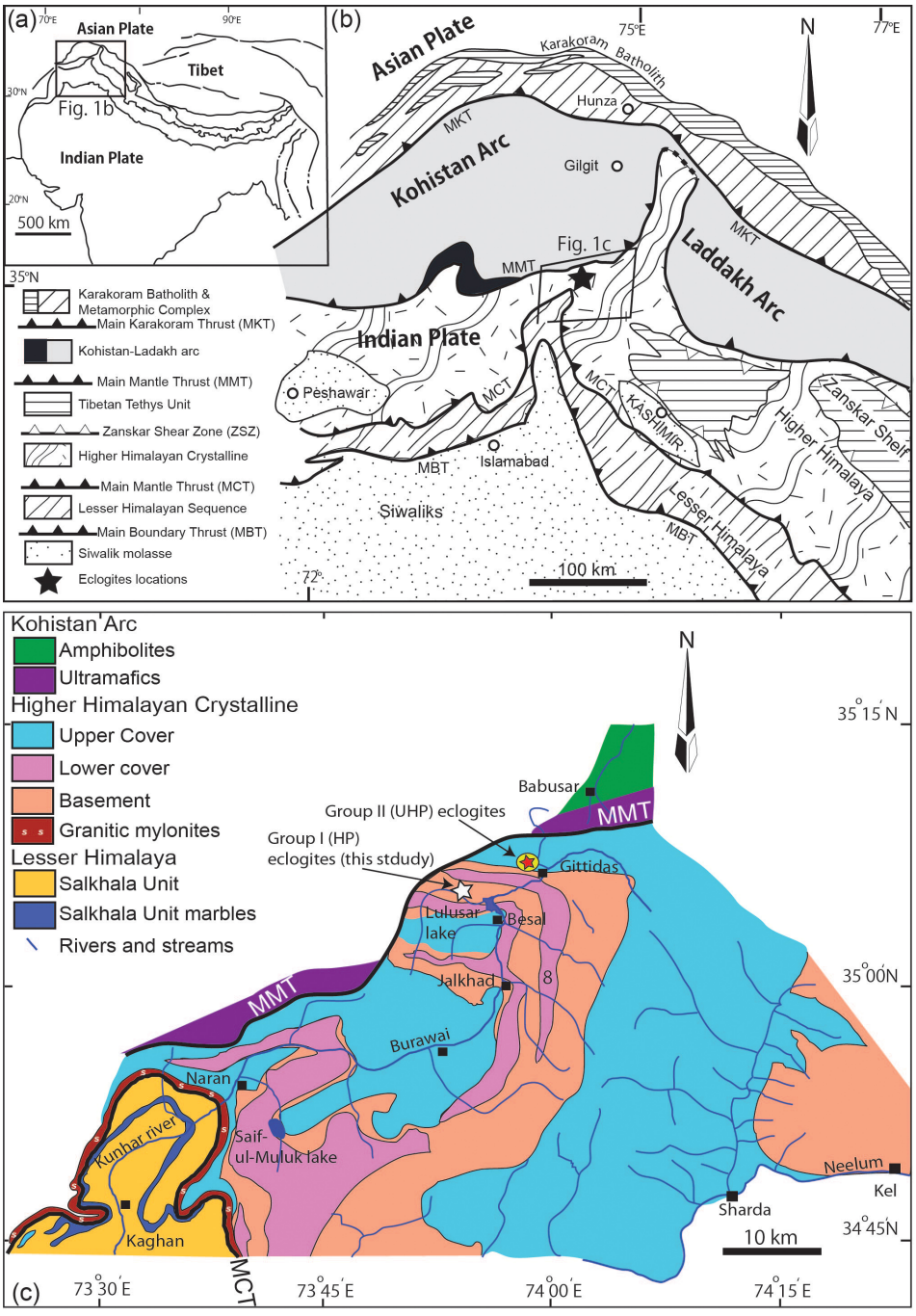

Figure 1. **(a)** Regional sketch showing the main tectonic units along the Himalayan region. **(b)** Enlarged portion of the area in western Himalaya displaying southern part of the Eurasian Plate in the north, Kohistan–Ladakh arcs in the middle, and Indian Plate lithologies in the south. **(c)** Simplified geological map of the Kaghan Valley, where the eclogites are exposed. White star represents HP eclogites from which zircon grains were investigated in this study. Also, the UHP eclogite (red star enclosed in a yellow circle) locality has been marked (map modified after Rehman et al., 2017, with references).

several grains (details on their magmatic origin are reported in Rehman et al., 2013a, 2016, 2018). In contrast, zircon grains in Group II eclogites yielded ^{235}U–^{207}Pb age values in the range 47.0 ± 11 Ma to 39.7 ± 8.7 Ma, with a concordant age of 44.9 ± 1.2 Ma (Rehman et al., 2013a), interpreted as metamorphic recrystallization/growth age during the India–Asia collision-related subduction and eclogite-facies metamorphism, on the basis of lower Th/U ratios (< 0.05), the presence of inclusions of garnet, omphacite, rare coesite, and rutile, and the preservation of sector or fir tree zoning (de-

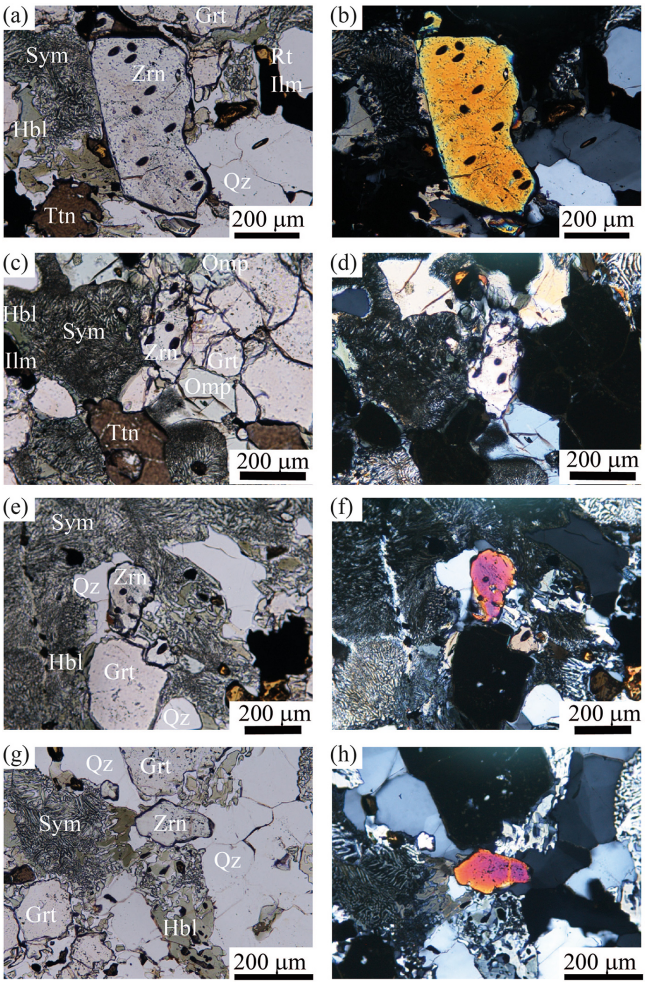

Figure 2. Photomicrographs of selected Himalayan Group I eclogite samples investigated here (images on the left are taken under plane-polarized light, those on the right under cross-polarized light), displaying textural features and occurrence of zircon grains. The dark elliptical holes on zircon grains represent the spots of previous HR-SIMS U–Pb isotope analyses. Abbreviations used are after Whitney and Evans (2010) except Sym, which stands for symplectites.

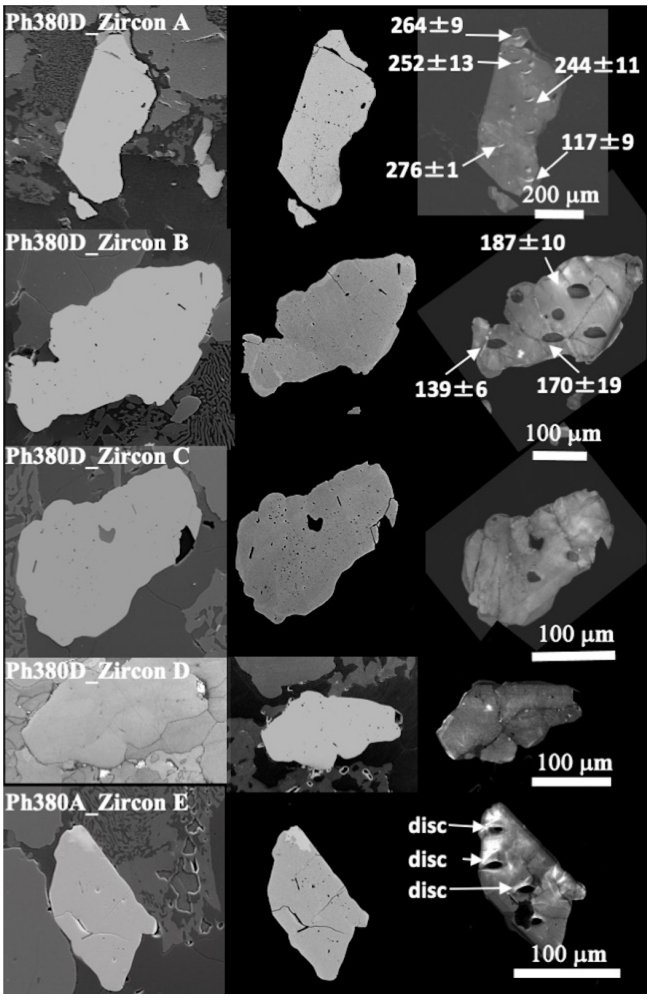

Figure 3. Secondary electron (left column), backscattered electron (middle column), and cathodoluminescence (right column) images of the studied zircon crystals. Elliptical holes in zircon grains show the spots of previous HR-SIMS U-Pb analyses, and relatively small and circular holes represent spots of trace-element analyses. Digits indicate U–Pb age (in Ma) with errors; "disc" means discordant.

tails on their metamorphic origin are reported in Rehman et al., 2013a, 2016, 2018). These data were consistent with the results reported by Spencer and Gebauer (1996) and Kaneko et al. (2003). It is interesting that the majority of zircon grains in Group I eclogites yielded concordant ages around 276 ± 2.4 Ma (see Fig. 10 in Rehman et al., 2013a) with several grains or domains within zircon grains that yielded age values of ca. 244 ± 11, 187 ± 10, 170 ± 19, and 139 ± 6 Ma. None of the analysed spots in zircon grains from Group I eclogites produce age data that could be linked to the Himalayan orogeny associated with the subduction-related eclogite-facies event. In addition, none of the metamorphic zircon grains from Group II eclogites provided protolith-related magmatic ages (Rehman et al., 2013a).

The current study is an extension of the past work, conducted in order to investigate in detail the internal structures of several selected zircon grains in Group I eclogites that were already analysed for U–Pb ages in our earlier studies. Those grains were analysed for their crystallographic orientation at micrometre scale using the EBSD technique, in order to visualize the internally deformed and undeformed domains. Following that, the crystallographically distinct domains were analysed via NanoSIMS for ^{238}U–^{206}Pb ages to find the effect of deformation on the geochronological record.

4 Methods

Analytical methods regarding thin-section preparation, polishing, petrography, and EBSD procedures are the same as those reported in Rehman et al. (2023). Five zircon grains from two polished thin sections from Group I eclogites were investigated for EBSD study, combined with NanoSIMS U–Pb isotope ages. After petrographical study and observations through BSE and CL imaging using scanning electron microscopy (SEM), the samples were analysed for EBSD with a scanning step size of 1–2 µm under an accelerating voltage of 17 kV and at a working distance of 25 mm. CamScan X500FE Crystal Probe at Géosciences Montpellier, Université de Montpellier, France, was used for the EBSD analyses. The data were obtained and cleaned using the HKL Aztec and Channel 5 software programs and processed with the MTEX 5.7.0, a MATLAB toolbox for quantitative textural analysis (Hielscher and Schaeben, 2008, available a: https://mtex-toolbox.github.io, last access: 23 September 2023). Band contrast images, EBSD phase maps, crystallographic orientation maps, orientation distribution function (ODF), and misorientations within single grains were reproduced via the MTEX toolbox, following the methods reported elsewhere (Bunge, 1982; Mainprice et al., 2011, 2015). Multi-spot analyses (38 spots on five selected zircon grains) of ^{238}U–^{206}Pb isotopes were conducted at the Atmosphere and Ocean Research Institute (AORI), The University of Tokyo, using the NanoSIMS 50. Spot size of individual analysis was about 10 µm in diameter. Analysis time for individual spot was 300 s, and during single analysis a set of ratios were measured. During analysis, geochemical standards used were NIST 610 glass and two zircon standards (zircon 91500 of crystallization age of 1065 Ma and zircon QGNG of crystallization age of 1850 Ma). Analytical results, isotope ratios, and 2σ errors are shown in Table 1. Common Pb corrections were made using the maximum age of crystallization obtained from each zircon grain, the ^{204}Pb/^{206}Pb ratios measured in each spot, divided by the value 0.0590 (calculated from the ^{204}Pb/^{206}Pb ratios obtained from the NIST610 standard glass and zircon 91500 during the analytical session, shown as f-com in Table 1). Uncertainties of the age data (shown in Table 1) were obtained from the instrumental calibration and are shown in absolute values. The ^{238}U–^{206}Pb age was calculated using the equation $t = 1/\lambda_{238} \ln((^{206}\mathrm{Pb}^*/^{238}\mathrm{U}) + 1)$, where ^{206}Pb*/^{238}U was calculated as $(1 - \text{f-com}) \times {}^{206}\mathrm{Pb}/{}^{238}\mathrm{U}$. Relatively higher values of f-com observed in several spots (data shown in bold in Table 1) suggest the presence of common Pb in those domains; hence the U–Pb age data for those spots are of low validity or indicate Pb loss. Other spots had low common Pb values that have an insignificant effect on U–Pb age.

5 Results

Details on individual zircon grains from the Himalayan eclogites are presented below.

5.1 Sample Ph380D_Zircon grain A

Zircon grain, labelled "A" in sample Ph-380D, is euhedral, surrounded predominantly by the symplectitic domain at one edge, and shares other edges with quartz, amphibole, and partly with garnet (Fig. 2). The grain is about 500 µm long and about 250 µm wide (Fig. 3). The BSE and CL images (Fig. 3) show homogeneous internal structure with no obvious zoning in the grain. Moreover, it contains numerous micro-inclusions of plagioclase, quartz, and apatite, suggesting its magmatic nature is still preserved. The EBSD phase map portrays *c* axis of the grain along the elongation direction, with local intra-grain misorientation up to 3° along the outer domain from the central domain (Fig. 4), and up to 15° to the mean orientation in the mapped area (Fig. 4). For this study, eight spots were analysed within this grain using NanoSIMS, and are shown as small circles with analyses nos. 19–26 (Fig. 4). Among those spots three spots (spot no. 20, no. 21, and no. 22; see Table 1) yielded ^{238}U–^{206}Pb isotope ages of 256.74 ± 51.59, 266.53 ± 35.15, and 291.28 ± 37.86 Ma, respectively. Two other spots (no. 24 and no. 25) showed age values of 237.59 ± 34.03 and 236.39 ± 38.41 Ma, and spot no. 26, located on the edge of the grain, yielded an age value of 145.49 ± 36.73 Ma. In addition, spot no. 19, located on the misoriented zone, yielded a significantly younger age value of 52.12 ± 4.47 Ma (Table 1).

5.2 Sample Ph380D_Zircon grain B

Zircon grain, labelled "B" in sample Ph-380D, is subhedral with some resorbed edges, also surrounded by symplectitic domain, and shares other edges with garnet, amphibole, and omphacite. This grain is about 400 µm long and about 200 µm wide (Fig. 3). The SEM, BSE, and CL images show homogeneous appearance, lack of internal zoning, and traces of several healed fractures which are visible on the CL image. The EBSD phase map (Fig. 4) portrays *c* axis of this grain also oriented along the elongation direction. Local intra-grain misorientation, up to 3°, is observed at several domains (Fig. 4), and misorientation to the mean orientation in the mapped area may reach 5° (Fig. 4). Three NanoSIMS-analysed spots on differently oriented domains in this grain give ^{238}U–^{206}Pb isotope ages of 119.67 ± 34.82, 161.81 ± 46.06, and 179.52 ± 43.73 Ma from spots no. 11, no. 12, and no. 13, respectively (Fig. 4 and Table 1).

5.3 Sample Ph380D_Zircon grain C

Zircon grain, labelled "C" in sample Ph-380D, displays features more or less similar to those observed in grain B; however, this grain shows much obvious misorientation at the

Table 1. NanoSIMS U–Pb isotope results of the analysed zircon grains.

Sequence	Sample & grain ID	$^{204}Pb/^{206}Pb$	Error (abs)	$^{206}Pb/^{238}U$	f-com	$^{206}Pb^*/^{238}U$	Error (abs)	^{238}U–^{206}Pb age (Ma)	Error (abs)
0829_19	**PH380D_A1**	**0.0512**	**0.0067**	**0.1240**	**0.9345**	**0.0081**	**0.0007**	**52.12**	**4.47**
0829_20	PH380D_A2	0.0000	0.0021	0.0405	0.0000	0.0405	0.0083	255.74	51.59
0829_21	PH380D_A3	0.0000	0.0008	0.0422	0.0000	0.0422	0.0057	266.53	35.15
0829_22	PH380D_A4	0.0019	0.0017	0.0479	0.0355	0.0462	0.0061	291.29	37.86
0829_23	**PH380D_A5**	**0.0067**	**0.0035**	**0.0353**	**0.1224**	**0.0310**	**0.0052**	**196.89**	**32.50**
0829_24	PH380D_A6	0.0016	0.0014	0.0387	0.0293	0.0375	0.0055	237.59	34.03
0829_25	PH380D_A7	0.0024	0.0025	0.0390	0.0432	0.0374	0.0062	236.39	38.41
0829_26	PH380D_A8	0.0000	0.0020	0.0228	0.0000	0.0228	0.0058	145.49	36.73
0829_27	PH380D_D1	0.0016	0.0010	0.0366	0.0288	0.0355	0.0047	225.18	29.10
0829_28	PH380D_D2	0.0018	0.0010	0.0335	0.0321	0.0324	0.0045	205.69	27.96
0829_29	PH380D_D3	0.0008	0.0007	0.0207	0.0154	0.0204	0.0040	130.22	25.51
0829_30	PH380D_D4	0.0031	0.0018	0.0243	0.0572	0.0229	0.0039	146.21	24.68
0829_31	PH380D_D5	0.0099	0.0023	0.0418	0.1801	0.0343	0.0072	217.35	45.12
0829_32	PH380D_D6	0.0006	0.0009	0.0424	0.0115	0.0419	0.0044	264.44	27.11
0829_33	PH380D_D7	0.0007	0.0006	0.0447	0.0133	0.0441	0.0042	278.37	25.99
0829_34	PH380D_D8	0.0038	0.0015	0.0285	0.0690	0.0265	0.0037	168.68	23.26
0829_35	**PH380D_C1**	**0.0065**	**0.0023**	**0.0246**	**0.1200**	**0.0216**	**0.0040**	**137.84**	**25.24**
0829_36	PH380D_C2	0.0012	0.0019	0.0233	0.0219	0.0228	0.0049	145.19	30.92
0829_37	PH380D_C3	0.0018	0.0030	0.0156	0.0335	0.0150	0.0054	96.20	34.53
0829_38	**PH380D_C4**	**0.0131**	**0.0063**	**0.0126**	**0.2411**	**0.0096**	**0.0033**	**61.52**	**21.38**
0829_39	PH380D_C5	0.0031	0.0021	0.0187	0.0569	0.0177	0.0047	112.82	29.97
0829_40	**PH380D_C6**	**0.0269**	**0.0042**	**0.0294**	**0.4974**	**0.0148**	**0.0029**	**94.56**	**18.32**
0829_41	**PH380D_C7**	**0.0135**	**0.0046**	**0.0098**	**0.2486**	**0.0073**	**0.0042**	**47.20**	**27.03**
0830_7	**PH380D_C8**	**0.0112**	**0.0042**	**0.0099**	**0.2069**	**0.0079**	**0.0032**	**50.51**	**20.62**
0830_8	PH380D_C9	0.0025	0.0015	0.0300	0.0466	0.0286	0.0072	181.99	44.81
0830_9	PH380D_C10	0.0000	0.0009	0.0176	0.0000	0.0176	0.0044	112.56	27.91
0830_10	**PH380D_C11**	**0.0085**	**0.0042**	**0.0177**	**0.1573**	**0.0149**	**0.0037**	**95.21**	**23.79**
0830_11	PH380D_B1	0.0063	0.0050	0.0212	0.1163	0.0187	0.0055	119.67	34.82
0830_12	PH380D_B2	0.0000	0.0074	0.0254	0.0000	0.0254	0.0073	161.81	46.06
0830_13	PH380D_B3	0.0000	0.0090	0.0282	0.0000	0.0282	0.0070	179.52	43.73
0830_14	**PH380A_E1**	**0.0072**	**0.0016**	**0.0215**	**0.1321**	**0.0186**	**0.0065**	**119.12**	**40.90**
0830_15	PH380A_E2	0.0054	0.0014	0.0237	0.0994	0.0214	0.0064	136.22	40.34
0830_16	PH380A_E3	0.0003	0.0004	0.0436	0.0050	0.0434	0.0070	273.60	43.24
0830_17	PH380A_E4	0.0007	0.0006	0.0316	0.0133	0.0312	0.0075	197.86	46.81
0830_18	PH380A_E5	0.0038	0.0014	0.0200	0.0700	0.0186	0.0066	119.10	41.86
0830_20	PH380A_E7	0.0019	0.0007	0.0427	0.0344	0.0412	0.0059	260.41	36.41

Data shown in bold, with relatively higher values of f-com (defined as fraction of common Pb), suggest the presence of common Pb; therefore, the U–Pb age data from those spots indicate Pb loss. Other spots had low common Pb values and thus have an insignificant effect on the U–Pb age.

intra-grain scale, which exceeds 5° (Fig. 4). In this grain, 11 spots (nos. 7–10 and nos. 35–41) were analysed for ^{238}U–^{206}Pb isotope ages on differently oriented domains using the NanoSIMS. The analysed data yield values between 182 and 47 Ma (Table 1, Fig. 4). The majority of those spots yield unclear age values except two spots (no. 7 and no.41) that yield ^{238}U–^{206}Pb isotope ages of 50.51 ± 20.62 and 47.20 ± 27.03 Ma (Table 1). Although the age data described here and displayed in Table 1 show relatively larger uncertainties, these large errors are due to the younger zircons and their lower U and Pb contents.

5.4 Sample Ph380D_Zircon grain D

Zircon grain, labelled "D" in sample Ph-380D, has well-developed crystal edges and appears as a homogeneous single crystal when viewed under the optical microscope (Fig. 2). However, it contains several healed cracks that cut across the grain when observed via CL imaging (Fig. 3). This grain is about 250 µm long and 150 µm wide (Fig. 3). The EBSD phase map portrays local misorientation up to 3° with respect to the middle part of the grain and up to 12° with respect to the mean orientation in the analysed area (Fig. 4). In this grain, eight NanoSIMS analyses for ^{238}U–^{206}Pb isotope ratios (spots nos. 27–34) were carried out on differently

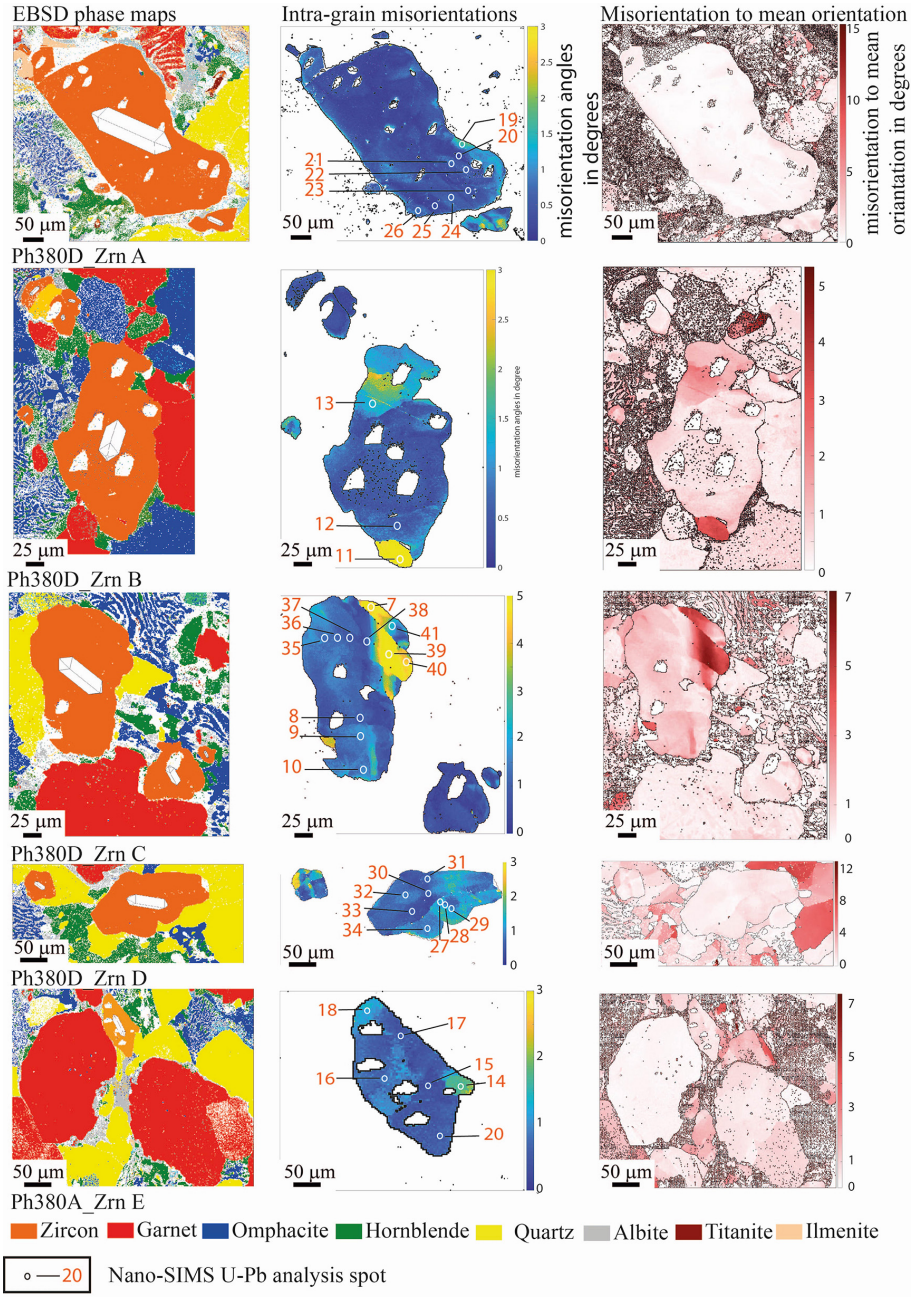

Figure 4. EBSD phase maps (left column), local misorientation within single zircon grains (middle column), and misorientations relative to the mean orientation within the EBSD analysed areas (right column). Zircon crystal shapes drawn on the EBSD phase maps show the orientation of the *c* axis along the elongation direction. Small white circles indicate spots of the NanoSIMS analyses, and the digits pointing to those circles are the analysis numbers as shown in Table 1. White empty regions in zircon grains are the ablated parts after the HR-SIMS U-Pb analyses. For other details on the internal misorientation and NanoSIMS age results, see text.

oriented domains (Table 1, Fig. 4). The analysed spots yield ages of 278.37 ± 25.99 and 264.44 ± 27.11 Ma from the core or middle domain, values of 225.18 ± 29.10, 217.35 ± 45.12, and 205.69 ± 27.96 Ma from the relatively undeformed domain, and three other spots (no. 29, no. 30, and no. 34), analysed on the slightly misoriented domains, give ^{238}U–^{206}Pb isotope ages of 130.22 ± 25.51, 146.21 ± 24.68, and 168.68 ± 23.26 Ma, respectively (Fig. 4).

5.5 Sample Ph380A_Zircon grain E

Zircon grain, labelled "E" in eclogite sample Ph-380A, is euhedral, shares sharp edges with surrounding minerals (gar-

net, quartz, symplectitic diopside, and amphibole), and is about 250 µm long and about 80 µm wide (Fig. 3). In BSE and CL images (Fig. 3), several fractures are visible in this grain. The EBSD phase map (Fig. 4) portrays a homogeneous pattern, displays sharp edges, and local misorientation is obvious through the orientation maps, showing at least three slightly different orientations within the single grain (Fig. 4). Internal misorientation is up to 3° with respect to the middle part of the grain (Fig. 4). NanoSIMS ^{238}U–^{206}Pb isotope analyses (small circles with number marked on Fig. 4, and results shown in Table 1) from two spots (no. 16 and no. 20) yield ages of ca. 273.60 ± 43.24 and 260.41 ± 36.41 Ma, respectively. Several other spots yield ^{238}U–^{206}Pb isotope age values between 119 and 198 Ma.

6 Discussion

Here, we present the geological information obtained from the Himalayan eclogites during past studies, their interpretations (Rehman et al., 2007, 2008, 2013a, 2016, 2023), and their link with the current research. An earlier study (Rehman et al., 2013a) conducted five analyses on zircon grain A for U–Th–Pb isotope ratios using a high-resolution secondary ionization mass spectrometer (HR-SIMS CAMECA IMS 1270). Four analyses on zircon grain A yielded ^{235}U–^{207}Pb ages of 276 ± 1, 264 ± 9, 252 ± 13, and 244 ± 11 Ma, respectively (data adopted from Rehman et al., 2013a, and shown in Fig. 3). The age data were interpreted as related to the Permian Panjal Trap magmatism. In addition, one analysis resulted in a ^{235}U–^{207}Pb age of 117 ± 9 Ma, which neither indicates protolith age nor represents eclogite-facies metamorphism. It is important to state that the geochronological results obtained from the investigated zircon grains via the HR-SIMS analyses are consistent with the age data obtained through the NanoSIMS analysis. In fact, the advantage of the NanoSIMS analytical technique is the increased spatial resolution, with an analytical spot size of < 10 µm. That small-scale analytical resolution allowed us to obtain geochronological details from multiple tiny domains within a single grain. Looking at the geochronological results, spot nos. 24 and 25 in zircon Grain A give somehow younger age values than the commonly identified age of the protolith emplacement (ca. 276 ± 2.4 Ma concordia age; Rehman et al., 2013a). Similarly, spot no. 26 in the same grain, yielding 145 Ma, possibly indicates geochronological resetting or Pb loss during the eclogite-facies metamorphism. Similarly, HR-SIMS ^{235}U–^{207}Pb isotope age values of 187 ± 10, 170 ± 19, and 139 ± 6 Ma were obtained from the three analysed spots (data shown in Fig. 3) in zircon Grain B. The data can neither be linked to the protolith formation, nor can they be associated with the metamorphic event in the Himalayan belt. These pieces of evidence suggest that Grain B was strongly reset and lost the protolith-related records. The majority of the analyses in zircon Grain C, except two, also suggest those domains were reset or affected during metamorphism and lost the records of the protolith-related magmatic event. One edge of the grain (where the other two spots, no. 7 and no. 41, were located) yields values of 50.51 ± 20.62 and 47.20 ± 27.03 Ma (Table 1). Those age data indicate recrystallization or growth of the analysed domains during the India–Asia collision and subduction-related UHP metamorphic event, well-known in the Himalayan metamorphic belt (Rehman et al., 2013a, 2016). Similarly, the geochronological values of 264.44 Ma from spot no. 32 and 278.37 Ma from spot no. 33 of zircon Grain D, obtained from the core and middle domains, most likely undeformed, are interpreted as the protolith-related magmatic event. Such age values are well-known to represent the Panjal Trap magmatism in the Himalayan region (e.g. Rehman et al., 2018). Three other spots (no. 27, no. 28, and no. 31), located on relatively undeformed domains in the same grain, showed comparatively younger values, due to Pb loss. Similar results (plotted on the concordia line but becoming younger toward the origin of the plot, for example Fig. 10 in Rehman et al., 2013a) were obtained from several zircon grains from Group I eclogites. In contrast, three other spots (no. 29, no. 30, and no. 34), analysed on the slightly misoriented domains, gave values of 130.22, 146.21, and 168.68 Ma, respectively, and are interpreted to have been affected by deformation. The fifth grain, zircon Grain E, was previously analysed by Rehman et al. (2013a) for four spots using the HR-SIMS (the elliptical holes in Fig. 3 show the bombarded spots). All the four analyses were discordant and did not give a geologically meaningful age. NanoSIMS analysis on undeformed domain in Grain E produced ages of 273.60 ± 43.24 and 260.41 ± 36.41 Ma from spot no. 16 and no. 20, respectively, which are interpreted as a protolith formation. In summary, the majority of the NanoSIMS-analysed spots yield geochronological results from the undeformed domains that are identical to previously reported age data (Rehman et al., 2013a, 2016) and represent the Permian Panjal Trap magmatism in the study area. Several spots from the EBSD-visualized deformed or relatively misoriented domains yield values between 119 and 198 Ma and can be interpreted as resulting from Pb loss or geological resetting. Moreover, the 52 and 47 Ma ages from the newly grown or strongly misoriented domain are linked to the India–Asia collision and the subduction-related eclogite-facies event in the Himalayan metamorphic belt. The absence or lack of domains younger than 47 Ma in the analysed grains indicates that an eclogite-facies stage was the last deformation or recrystallization event that could reset the magmatic records in the studied zircons.

7 Implications of the EBSD data on geologically meaningful geochronology

Crystal plastic deformation in zircon grains and its effects on geochronology have been attributed to shearing and my-

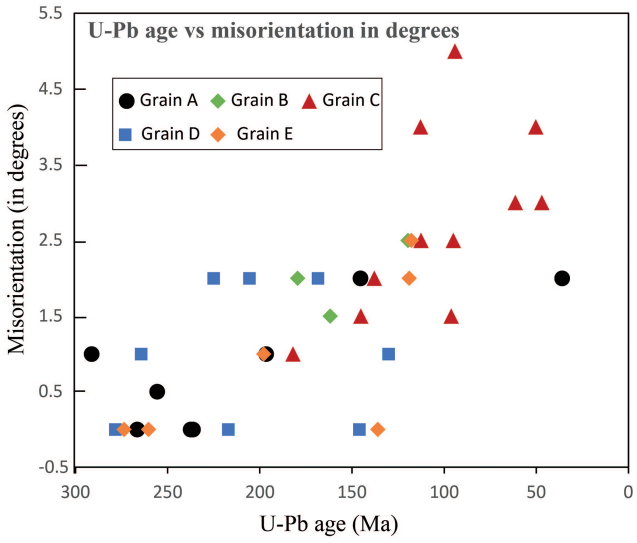

Figure 5. Plot showing the U–Pb age (Ma) versus internal misorientation (in degrees) of the EBSD- and NanoSIMS-analysed zircon grains. Note that the Permian age of magmatic emplacement of the protoliths of the studied eclogites (Panjal Trap magmatism) is retained in the homogeneous zircon domains (with misorientation $< 1^\circ$ and U–Pb ages of 279–250 Ma), whereas relatively deformed domains (with several degrees of misorientation) show younger or affected ages.

lonitization by a number of researchers (e.g. Reddy et al., 2007; Timms and Reddy, 2009; Kaczmarek et al., 2011; Piazolo et al., 2012; Kusiak et al., 2013; Kovaleva et al., 2014, 2016, 2017, 2018, 2021; Seydoux-Guillaume et al., 2015). Kovaleva et al. (2018) discussed possible mechanisms of deformation in zircon grains in deformed and shear zones that were interpreted to have accumulated strain through elastic deformation, fracturing, geometrically necessary dislocations (GNDs), and low-energy migration creeps, which had been reported in several earlier studies (e.g. Hobbs, 1968; Poirier, 1985; Kaczmarek et al., 2011; Kovaleva et al., 2014, 2016). Generally, dislocations in zircon grains, as well as in other minerals, are determined through TEM investigation (Leroux et al., 1999), via EBSD maps constructed from the weighted Burgers vector calculations (Wheeler et al., 2009, 2012; MacDonald et al., 2013; Kovaleva et al., 2018), and boundary geometry with respect to the crystallographic orientations of the zircon grains analysed via EBSD mapping (e.g. Reddy et al., 2007; Kovaleva et al., 2014, 2018). The majority of these studies targeted strongly sheared and mylonitized metamorphic rocks. So far, no study has been conducted on intra-grain plastic deformation in zircon grains that crystallized/recrystallized in eclogite facies metamorphic rocks.

In this study, we focused on zircon grains present in the Himalayan eclogites. The studied grains preserve magmatic records of their protoliths (Panjal Trap basalts). Later, the mafic rocks were subducted together with the continental crustal lithologies to upper-mantle depths and transformed into HP/UHP eclogite-facies rocks. The majority of these zircon grains contain inclusions of plagioclase, quartz, biotite, and ilmenite in their core. They exhibit high Th/U ratios (> 0.3), yielded a concordant age of ca. 267.1 ± 2.4 Ma, and were interpreted to have crystallized during the Permian Panjal Trap magmatism (Rehman et al., 2013a, 2016, 2018). Similarly, numerous zircon grains from Group II eclogites, which show sector zoning and contain inclusions of garnet, clinopyroxene, rutile, and coesite, have a relatively low Th/U ratio (< 0.05). They yielded a U–Pb concordant age of ca. 44.9 ± 1.2 Ma and were interpreted to have recrystallized from their magmatic precursors during the Eocene UHP eclogite-facies event when the Indian Plate subducted beneath the Eurasian Plate and reached mantle depths exceeding 90 km (coesite-stability field; for details see Rehman et al., 2013a).

Several zircon grains or domains within grains show U–Pb age data scattering between 230 and 106 Ma. These anomalous data suggest deformation-related resetting or Pb loss in such domains. To resolve this issue, we focused on analysing several zircon grains for EBSD and then re-dating the crystallographically distinct domains (deformed and undeformed) using NanoSIMS. Except for some healed cracks in two grains, there were no clearly deformed domains that could be identified via normal optical investigations or through BSE and CL imaging. However, when the EBSD-generated orientation maps were acquired, several local domains within single grain appeared plastically deformed, showing intragrain misorientations. Such micro-scale deformed or geologically reset domains are generally impossible to identify through the commonly used methods (e.g. under optical microscope, BSE, and CL). It is known that shearing and mylonitization that is pervasive in host rocks likely reset the geochemical (redistribution of trace elements and isotopes) and geochronological records in zircon grains that are found in those rocks. In fact, EBSD mapping has proved that strains at low-angle boundaries, tilt dislocations, and rotation axis were the common mechanisms of deformation that generally reset the geochemical and geochronological records in zircon grains (e.g. Piazolo et al., 2012; Kovaleva et al., 2017, 2018).

The studied zircon grains showed local misorientations at the grain boundaries. These local domains show variable geochronological results from a single grain. The strained domains therefore confirm that plastic deformation in zircon grains has the potential to be the main factor in re-equilibrating the geochronological records. This study confirms that plastic deformation in zircon grains is not only attributed to the strong shearing and mylonitization in metamorphic rocks, but that high P–T equilibration conditions also play a significant role in plastic deformation and resetting of geochemical and geochronological records in zircon grains, which are generally considered hard and resistant to chemical modifications. It is therefore suggested that simple optical microscopy and BSE/CL imaging are not enough

to identify internal structures to select potential domains for geochemical analyses. In addition, EBSD mapping is recommended to visualize geologically reset domains before any destructive methods (e.g. laser ablation) are used to analyse key zircon samples.

This study provides clear evidence of the effect of plastic deformation on the U–Pb isotope system in zircons recovered from HP/UHP eclogites (Fig. 5). As mentioned above, the studied Himalayan eclogites show no pervasive deformation or foliation visible through the textural observations. However, EBSD data from the entire thin sections (Rehman et al., 2023) were characterized by an L-type fabric in omphacite showing strongly preferred orientation along the [001] or *c* axis and a complex fabric with no distinct pattern in garnet. The L-type fabric of omphacite was interpreted to result from the deformation of eclogites during high *P*–*T* prograde metamorphism when the protolith rocks (basalts) were subducted to mantle depths and transformed into eclogites. The studied zircon grains in those eclogites preserve the magmatic records of the protolith in the undeformed domains that display no internal misorientations despite having undergone HP eclogite-facies metamorphism. However, several-degree misoriented domains in the studied zircon grains show anomalous age values (Fig. 5) that could be attributed to ductile deformation possibly initiated under relatively high *P*–*T* metamorphic conditions, which likely caused geological/geochemical resetting in these grains. This study indicates that zircon grains undergo plastic deformation under relatively high *P*–*T* metamorphic conditions even in texturally non-foliated metamorphic rocks; therefore care must be taken to identify pristine domains in zircon grains before applying any destructive geochemical analyses.

Data availability. Raw data can be provided by the corresponding author upon request.

Author contributions. HUR planned the project, conducted field work, and collected samples. HY conducted fieldwork and helped in sample preparation. FB and DM helped with EBSD analyses and data interpretation. TK, NT, and YS helped with NanoSIMS analyses. HUR wrote the manuscript draft and prepared all the illustrations. TK, NT, YJ, FB, DM, and HY revised and edited the manuscript.

Competing interests. The contact author has declared that none of the authors has any competing interests.

Disclaimer. Publisher's note: Copernicus Publications remains neutral with regard to jurisdictional claims made in the text, published maps, institutional affiliations, or any other geographical representation in this paper. While Copernicus Publications makes every effort to include appropriate place names, the final responsibility lies with the authors.

Special issue statement. This article is part of the special issue "(Ultra)high-pressure metamorphism, from crystal to orogenic scale". It is a result of the 14th International Eclogite Conference (IEC-14) held in Paris and Lyon, France, 10–13 July 2022.

Acknowledgements. EBSD analyses, at the Géosciences Montpelier, were supported by the Institut National des Sciences de l'Univers (INSU) du Centre National de la Recherche Scientifique (CNRS, France). NanoSIMS analyses were supported by the Atmosphere and Ocean Research Institute, The University of Tokyo, Kashiwa, Japan. We thank associate editor, Gaston Godard, and editor-in-chief Christian Chopin, for the through review, providing useful suggestions to improve the contents of this study and encouragement related to this contribution. We also are thankful for the critical comments of Klaus Mezger, Florian Hofmann, Dirk Spengler, and an anonymous reviewer that significantly improved the text, results, and their interpretations. English language was improved by Bo Causer of Kagoshima University, which we appreciate.

Financial support. Part of the research was supported by the Kagoshima University's Young Researchers Visiting Program and partly by the JSPS Kakenhi (grant nos. 15K05316 and 20K004135 to Hafiz U. Rehman).

Review statement. This paper was edited by Gaston Godard and reviewed by Klaus Mezger, Florian Hofmann, Dirk Spengler, and one anonymous referee.

References

Belousova, E. A., Griffin, W. L., O'Reilly, S. Y., and Fisher, N. I.: Igneous zircon: trace element composition as an indicator of source rock type, Contrib. Mineral. Petr., 143, 602–622, https://doi.org/10.1007/s00410-002-0364-7, 2002.

Bunge, H. J.: Texture analysis in materials science: mathematical methods, Butterworths publishers, Elseveir, London, https://doi.org/10.1016/C2013-0-11769-2, 1982.

Cherniak, D. J. and Watson, E. B.: Diffusion in zircon, Rev. Mineral. Geochem., 53, 113–139, https://doi.org/10.2113/0530113, 2003.

Hielscher, R. and Schaeben, H.: A novel pole figure inversion method: specification of the MTEX algorithm, J. App. Cryst., 41, 1024–1037, https://doi.org/10.1107/S0021889808030112, 2008.

Hobbs, B. E.: Recrystallization of single crystals of quartz, Tectonophysics, 6, 353–401, https://doi.org/10.1016/0040-1951(68)90056-5, 1968.

Kaczmarek, M. A., Reddy, S. M., and Timms, N. E.: Evolution of zircon deformation mechanisms in a shear zone (Lanzo massif, Western-Alps), Lithos, 127, 414–426, https://doi.org/10.1016/j.lithos.2011.09.016, 2011.

Kaneko, Y., Katayama, I., Yamamoto, H., Misawa, K., Ishikawa, M., Rehman, H. U., Kausar, A. B., and Shiraishi, K.: Timing of Himalayan ultrahigh-pressure metamorphism: sinking rate and subduction angle of the Indian continental crust beneath Asia, J. Metamorph. Geol., 21, 589–599, https://doi.org/10.1046/j.1525-1314.2003.00466.x, 2003.

Kovaleva, E. and Klötzli, U.: NanoSIMS study of seismically deformed zircon: evidence of Y, Yb, Ce and P redistribution and resetting of radiogenic Pb, Am. Mineral., 102, 1311–1327, https://doi.org/10.2138/am-2017-5975, 2017.

Kovaleva, E., Klötzli, U., Habler, G., and Libowitzky, E.: Finite lattice distortion patterns in plastically deformed zircon grains, Solid Earth, 5, 1099–1122, https://doi.org/10.5194/se-5-1099-2014, 2014.

Kovaleva, E., Klötzli, U., and Habler, G.: On the geometric relationship between deformation microstructures in zircon and the kinematic framework of the shear zone, Lithos, 262, 192–212, https://doi.org/10.1016/j.lithos.2016.07.001, 2016.

Kovaleva, E., Klötzli, U., Habler, G., Huet, B., Guan, Y., and Rhede, D.: The effect of crystal-plastic deformation on isotope and trace element distribution in zircon: combined BSE, CL, EBSD, FEG-EMPA and NanoSIMS study, Chem. Geol., 450, 183–198, https://doi.org/10.1016/j.chemgeo.2016.12.030, 2017.

Kovaleva, E., Klötzli, U., Wheeler, J., and Habler, G.: Mechanisms of strain accommodation in plastically-deformed zircon under simple shear deformation conditions during amphibolite-facies metamorphism, J. Struct. Geol., 107, 21–24, https://doi.org/10.1016/j.jsg.2017.11.015, 2018.

Kovaleva, E., Kusiak, M. A., Kenny, G. G., Whitehouse, M. J., Habler, G., Schreiber, A., and Wirth, R.: Nano-scale investigation of granular neoblastic zircon, Vredefort impact structure, South Africa: Evidence for complete shock melting, Earth Planet. Sc. Lett., 565, 116948, https://doi.org/10.1016/j.epsl.2021.116948, 2021.

Kusiak, M. A., Whitehouse, M. J., Wilde, S. A., Nemchin, A. A., and Clark, C.: Mobilization of radiogenic Pb in zircon revealed by ion imaging: implications for early Earth geochronology, Geology, 41, 291–294, https://doi.org/10.1130/G33920.1, 2013.

Leroux, H., Reimold, W. U., Koeberl, C., Hornemann, U., and Doukhan, J. C.: Experimental shock deformation in zircon: a transmission electron microscopic study, Earth Planet. Sc. Lett., 169, 291–301, https://doi.org/10.1016/S0012-821X(99)00082-5, 1999.

MacDonald, J. M., Wheeler, J., Harley, S. L., Mariani, E., Goodenough, K. M., Crowley, Q., and Tatham, D.: Lattice distortion in a zircon population and its effects on trace element mobility and U–Th–Pb isotope systematics: examples from the Lewisian Gneiss Complex, northwest Scotland, Contrib. Mineral. Petr., 166, 21–41, https://doi.org/10.1007/s00410-013-0863-8, 2013.

Mainprice, D., Hielscher, R., and Schaeben, H.: Calculating anisotropic physical properties from texture data using the MTEX open source package, in: Deformation Mechanisms, Rheology and Tectonics: Microstructures, Mechanics and Anisotropy, edited by: Prior, D. J., Rutter, E. H., and Tatham, D. J., Geological Society London Special Publications, 360, 175–192, https://doi.org/10.1144/SP360.10, 2011.

Mainprice, D., Bachmann, F., Hielscher, R., and Schaeben, H.: Descriptive tools for the analysis of texture projects with large datasets using MTEX: strength, symmetry and components, in: Rock deformation from Field, Experiments and Theory: A volume in Honour of Ernie Rutter, edited by: Faulkner, D. R., Mariani, E., and Mechlenburgh, J., Geological Society of London Special Publications, 409, 251–271, https://doi.org/10.1144/SP409.8, 2015.

O'Brien, P. J., Zotov, N., Law, R., Khan, M. A., and Jan, M. Q.: Coesite in Himalayan eclogite and implications for models of India–Asia collision, Geology, 29, 435–438, https://doi.org/10.1130/0091-7613(2001)029<0435:CIHEAI>2.0.CO;2, 2001.

Piazolo, S., Austrheim, H., and Whitehouse, M.: Brittle-ductile microfabrics in naturally deformed zircon: deformation mechanisms and consequences for U-Pb dating, Am. Mineral., 97, 1544–1563, https://doi.org/10.2138/am.2012.3966, 2012.

Poirier, J. P.: Creep of Crystals: High-temperature Deformation Processes in Metals, Ceramics and Minerals, Cambridge University Press, New York, https://doi.org/10.1017/CBO9780511564451, 1985.

Reddy, S. M., Timms, N. E., Trimby, P., Kinny, P. D., Buchan, C., and Blake, K.: Crystal plastic deformation of zircon: a defect in the assumption of chemical robustness, Geology, 34, 257–260, https://doi.org/10.1130/G22110.1, 2006.

Reddy, S. M., Timms, N. E., Pantleon, W., and Trimby, P.: Quantitative characterization of plastic deformation of zircon and geological implications, Contrib. Mineral. Petr., 153, 625–645, https://doi.org/10.1007/s00410-006-0174-4, 2007.

Reddy, S. M., Timms, N. E., Hamilton, P. J., and Smyth, H. R.: Deformation-related microstructures in magmatic zircon and implications for diffusion, Contrib. Mineral. Petr., 157, 231–244, https://doi.org/10.1007/s00410-008-0331-z, 2009.

Rehman, H. U.: Geochronological enigma of the HP–UHP rocks in the Himalayan orogen, in: HP–UHP Metamorphism and Tectonic Evolution of Orogenic Belts, edited by: Zhang, L. F., Schertl, H.-P., and Wei, C. J., Geological Society of London Special Publication, 474, 183–207, https://doi.org/10.1144/SP474.14, 2019.

Rehman, H. U., Yamamoto, H., Kaneko, Y., Kausar, A. B., Murata, M., and Ozawa, H.: Thermobaric structure of the Himalayan metamorphic belt in Kaghan Valley, Pakistan, J. Asian Earth Sci. 29, 390–406, https://doi.org/10.1016/j.jseaes.2006.06.002, 2007.

Rehman, H. U., Yamamoto, H., Nakamura, E., Khalil, M. A., Zafar, M., and Khan, T.: Metamorphic history and tectonic evolution of the Himalayan UHP eclogites in Kaghan Valley, Pakistan, J. Miner. Petrol. Sci., 103, 242–254, https://doi.org/10.2465/jmps.080222, 2008.

Rehman, H. U., Kobayashi, K., Tsujimori, T., Ota, T., Yamamoto, H., Nakamura, E., Kaneko, Y., Khan, T., Terabayashi, M., Yoshida, K., and Hirajima, T.: Ion microprobe U–Th–Pb geochronology and study of micro-inclusions in zircon from the Himalayan high and ultrahigh-pressure eclogites, Kaghan Valley of Pakistan, J. Asian Earth Sci., 63, 179–196, https://doi.org/10.1016/j.jseaes.2012.04.025, 2013a.

Rehman, H. U., Yamamoto, H., and Shin, K.: Metamorphic *P-T* evolution of high-pressure eclogites from garnet growth and reaction textures: insights from the Kaghan Valley transectIon, northern Pakistan, Island Arc., 22, 4–24, https://doi.org/10.1111/iar.12010, 2013b.

Rehman, H. U., Lee, H. Y., Chung, S. L., Khan, T., O'Brien, P. J., and Yamamoto, H.: Source and mode of the Per-

mian Panjal Trap magmatism: Evidence from zircon U-Pb and Hf isotopes and trace element data from the Himalayan ultrahigh-pressure rocks, Lithos, 260, 286–299, https://doi.org/10.1016/j.lithos.2016.06.001, 2016.

Rehman, H. U., Jan, M. Q., Khan, T., Yamamoto, H., and Kaneko, Y.: Varieties of the Himalayan eclogites: A pictorial review of textural and petrological features, Island Arc., 26, e12209, https://doi.org/10.1111/iar.12209, 2017.

Rehman, H. U., Kitajima, K., Valley, J. W., Lee H. Y., Chung, S. L., Yamamoto, H., and Khan, T.: Low-δ^{18}O mantle-derived magma in Panjal traps overprinted by hydrothermal alteration and Himalayan UHP metamorphism: Revealed by SIMS zircon analysis, Gondwana Res., 56, 12–22, https://doi.org/10.1016/j.gr.2017.12.004, 2018.

Rehman, H. U., Iizuka, Y., Lee, H. Y., Chung, S. L., Duan, Z., Wei, C., Khan, T., Zafar, T., and Yamamoto, H.: Zirconium in rutile thermometry of the Himalayan ultrahigh-pressure eclogites and their retrogressed counterparts, Kaghan Valley, Pakistan, Lithos, 344–345, 86–99, https://doi.org/10.1016/j.lithos.2019.06.017, 2019.

Rehman, H. U., Mainprice, D., Barou, F., Yamamoto, H., Wei, C., Zafar, T., and Khan, T.: Crystallographic preferred orientations and microtexture of the Himalayan eclogites revealing records of syn-deformation peak metamorphic stage and subsequent exhumation, J. Struct. Geol., 167, 104792, https://doi.org/10.1016/j.jsg.2023.104792, 2023.

Seydoux-Guillaume, A.-M., Bingen, B., Paquette, J.-L., and Bosse, V.: Nanoscale evidence for uranium mobility in zircon and the discordance of U–Pb chronometers, Earth Planet. Sc. Lett., 409, 43–48, https://doi.org/10.1016/j.epsl.2014.10.044, 2015.

Spencer, D. A. and Gebauer, D.: SHRIMP evidence for a Permian protolith age and a 44 Ma metamorphic age for the Himalayan eclogites (Upper Kaghan, Pakistan): Implication for the subduction of the Tethys and the subdivision terminology of the NW Himalaya: Himalayan–Karakoram–Tibet Workshop, 11th, (Flagstaff, Arizona, USA), Abstract Volume, 147–150, 1996.

Spencer, D. A., Tonarini, S., and Pognante, U.: Geochemical and Sr–Nd isotopic characterization of Higher Himalayan eclogites (and associated metabasites), Eur. J. Mineral., 7, 89–102, 1995.

Timms, N. E. and Reddy, S. M.: Response of cathodoluminescence to crystal-plastic deformation in zircon, Chem. Geol., 261, 11–23, https://doi.org/10.1016/j.chemgeo.2008.09.008, 2009.

Whitney, D. L. and Evans, B. W.: Abbreviations for names of rock-forming minerals, Am. Mineral., 95, 185–187, https://doi.org/10.2138/am.2010.3371, 2010.

Wilke, F. D. H., O'Brien, P. J., Gerdes, A., Timmerman, M. J., Sudo, M., and Khan, M. A.: The multistage exhumation history of the Kaghan Valley UHP series, NW Himalaya, Pakistan from U-Pb and ^{40}Ar/^{39}Ar ages, Eur. J. Mineral., 22, 703–719, https://doi.org/10.1127/0935-1221/2010/0022-2051, 2010.

Wheeler, J., Mariani, E., Piazolo, S., Prior, D. J., Trimby, P., and Drury, M. R.: The Weighted Burgers Vector: a new quantity for constraining dislocation densities and types using Electron Backscatter Diffraction on 2D sections through crystalline materials, J. Microsc., 233, 482–494, https://doi.org/10.1111/j.1365-2818.2009.03136.x, 2009.

Wheeler, J., Mariani, E., Piazolo, S., Prior, D. J., Trimby, P., and Drury, M. R.: The Weighted Burgers Vector: a quantity for constraining dislocation densities and types using Electron Backscatter Diffraction on 2D sections through crystalline materials, Mater. Sci. Forum, 715–716, 732–736, https://doi.org/10.4028/www.scientific.net/MSF.715-716.732, 2012.